


A Case Study of the Weather Research and Forecasting Model Applied to the Joint Urban 2003 Tracer Field Experiment. Part 1: Wind and Turbulence

Matthew A. Nelson¹  · Michael J. Brown¹ · Scot A. Halverson¹ · Paul E. Bieringer² · Andrew Annunzio³ · George Bieberbach² · Scott Meech⁴

Received: 20 October 2014 / Accepted: 10 September 2015 / Published online: 25 September 2015
© Springer Science+Business Media Dordrecht (outside the USA) 2015

Abstract Numerical-weather-prediction models are often used to supply the mean wind and turbulence fields for atmospheric transport and dispersion plume models as they provide dense horizontally- and vertically-resolved geographic coverage in comparison to typically sparse monitoring networks. Here, the Weather Research and Forecasting (WRF) model was run over the month-long period of the Joint Urban 2003 field campaign conducted in Oklahoma City and the simulated fields important to transport and dispersion models were compared to measurements from a number of sodars, tower-based sonic anemometers, and balloon soundings located in the greater metropolitan area. Time histories of computed wind speed, wind direction, turbulent kinetic energy (e), friction velocity (u_*), and reciprocal Obukhov length ($1/L$) were compared to measurements over the 1-month field campaign. Vertical profiles of wind speed, potential temperature (θ), and e were compared during short intensive operating periods. The WRF model was typically able to replicate the measured diurnal variation of the wind fields, but with an average absolute wind direction and speed difference of 35° and 1.9 m s^{-1} , respectively. Using the Mellor-Yamada-Janjic (MYJ) surface-layer scheme, the WRF model was found to generally underpredict surface-layer TKE but overpredict u_* that was observed above a suburban region of Oklahoma City. The TKE-threshold method used by the WRF model's MYJ surface-layer scheme to compute the boundary-layer height (h) consistently overestimated h derived from a θ gradient method whether using observed or modelled θ profiles.

Keywords Atmospheric surface-layer winds · Turbulence · Urban transport and dispersion · Vertical structure · Weather Research and Forecasting

✉ Matthew A. Nelson
nelsonm@lanl.gov

¹ Los Alamos National Laboratory, MS F609, PO Box 1663, Los Alamos, NM 87545, USA

² Aeris, 1723 Madison CT, Louisville, CO 80027, USA

³ Citadel, 131 South Dearborn Street, Chicago, IL 60603, USA

⁴ Science and Technology in Atmospheric Research (STAR) LLC, 3125 Sterling Circle, Suite 107, Boulder, CO 80301, USA

1 Introduction

Atmospheric plume models require wind speed, wind direction, atmospheric stability, boundary-layer depth and/or turbulence input parameters in order to accurately predict the transport and dispersion of contaminants released within the atmospheric boundary layer (e.g., Pasquill and Smith 1984; Arya 1999). The input data used to drive atmospheric transport and dispersion models are typically acquired from the nearest surface meteorological station(s). In regions of spatially heterogeneous surface characteristics that directly affect the microscale meteorology (urban, coastal, complex terrain, etc.) it can be difficult to find observations that are representative of the local neighbourhood-scale conditions due to the typical separation of tens to hundreds of km between properly sited observation stations. Furthermore, standard weather stations rarely provide direct measurements of surface-layer turbulence and stability parameters such as the friction velocity (u_*), turbulent kinetic energy (e), surface heat flux, and Obukhov length (L), which are utilized by advanced atmospheric transport and dispersion models to determine the turbulent diffusion of the plume. The spatial density of sodar, radar, and balloon sounding networks that are used to measure the vertical structure is even more sparse. In the case of balloon soundings, measurements are typically obtained at 12-h intervals. Thus, the boundary-layer height (h), which is often used by atmospheric transport and dispersion models to account for vertical structure effects in the atmosphere, must often be approximated based on generalized diurnal cycle behaviour and may or may not account for local meteorological conditions at the time in question. A commonly used approach to address the issue of spatial and temporal limitations in atmospheric measurements is to use numerical-weather-prediction (NWP) models to fill in the gaps. Mesoscale NWP models such as the Weather Research and Forecast (WRF) model are being used to provide input data for microscale transport and dispersion simulations (e.g., Tewari et al. 2010; Chen et al. 2011; Wyszogrodzki et al. 2012).

Successful application of a plume dispersion model in an urban region requires that the NWP model produce the heterogeneous wind and turbulence fields that develop as a result of the spatially-varying urban canopy. As the airflow undergoes transition from rural conditions to the urban core, h grows due to the increasing surface roughness and subsequent enhanced near-surface turbulence and velocity deficit. A wake develops downwind of the urban core as the effects of the large buildings on the velocity and turbulence (as well as many other quantities that have smaller effects on transport and dispersion) fields mix with the prevailing flow and eventually undergo transition back to the ambient rural conditions. Due to the coarse horizontal resolution typically employed by mesoscale models, only the bulk flow and turbulence representing the horizontal average over the grid cell can be simulated. Therefore, many mesoscale models have implemented urban canopy parametrizations in order to account for the subgrid effects of buildings on the momentum, turbulence and thermal energy budgets (see reviews by Brown 2001 and Martilli 2007). The WRF model has implemented the Kusaka and Kimura (2004) single-layer urban canopy model to approximate these urban effects.

In this paper, we provide an analysis of the WRF model's ability to reproduce the prevailing wind speed, wind direction, and turbulence variables over the 1-month period of the Joint Urban 2003 (JU2003) field experiment, as well as analysis of the vertical structure of the boundary layer over a few individual 1-h time periods that coincide with plume dispersion experiments. Although there have been several comparative studies between mesoscale NWP model simulations and JU2003 field data (Liu et al. 2006; Niyogi et al. 2006; Chen et al. 2007, 2011; Wyszogrodzki et al. 2012), they primarily provide analyses of a wide variety of meteorological quantities over a few relatively short time periods. In addition to examining

a few 1-h time periods, we quantify the error in the WRF model's simulated fields that most affect atmospheric transport and dispersion: mean velocity, turbulence, and stability. This was done by examining time-series comparisons of these quantities predicted by the WRF model and observations over the course of the entire month of July 2003 at two locations that should be representative of the ambient conditions around the urban core. In Part 2 (Nelson et al. 2015, in review), tracer-gas measurements from the JU2003 field experiment will be used to evaluate how the WRF model data and turbulence assimilation schemes affect the urban transport and dispersion model calculations.

2 Experimental Overview

The JU2003 field tracer campaign took place from 29 June through 30 July 2003 in Oklahoma City, Oklahoma, USA for the purpose of evaluating urban dispersion models (Allwine et al. 2004; Brown et al. 2004). Oklahoma City provided a relatively large urban area devoid of major natural topographical features. The centre of the urban core of Oklahoma City has an average building height of approximately 50 m, with some buildings reaching 120 m in height (Burian et al. 2003), while the surroundings are suburban with significant tree-canopy coverage.

A wide range of meteorological instrumentation was deployed throughout the greater metropolitan area, including sodars, instrumented towers, and rawinsonde balloon soundings that provided vertical profiles of relevant quantities within the planetary boundary layer. Figure 1 shows the locations of the subset of wind instruments deployed in and around the urban core of Oklahoma City during JU2003 that are used in this analysis. Tables 1 and 2 provide the geographic locations, operating institution, and the measurement heights for the sodars and sonic anemometer towers, respectively. Time series of the mean wind and turbulence measurements from the Pacific Northwest National Laboratory (PNNL) sodar and Indiana University (IU) sonic tower, respectively, are used to evaluate the WRF model results over the entire month of July.

In addition to the meteorological instruments that were deployed throughout the duration of the JU2003 experiment, there were ten 8-h intensive operating periods (IOPs) when atmospheric transport and dispersion experiments were performed and additional meteorological observations were made including balloon sounding launches. Six IOPs were conducted during daytime hours and the remaining four IOPs were performed during the night. Here we have chosen to focus on four 2-h observation windows associated with four plume releases from three different IOPs (see Table 3). This was done in order to investigate the vertical structure of the atmospheric boundary layer over the suburban area of Oklahoma City. IOP2-R1 and IOP2-R3 both represent daytime cases in which the wind direction varied significantly over the 2-h period, 40° in the former case, and 50° in the latter. On the other hand, the daytime case IOP6-R1 and the nighttime case IOP8-R2 represent time periods in which the wind direction did not vary significantly over the 2-h period. The wind directions for IOP2-R1 were predominately from the south-west, while they were more southerly for IOP2-R3 and IOP6-R1, and south-easterly for IOP8-R2. The wind speeds were greatest for IOP8-R2.

Note that mean and turbulence statistics derived from the sonic data were computed using a 30-min running window that should be sufficient to include the fluctuations in frequencies above the spectral energy gap (Stull 1988). Much of the sonic and sodar observational data presented here are 1-h averages to match the output frequency of the WRF model simulations.

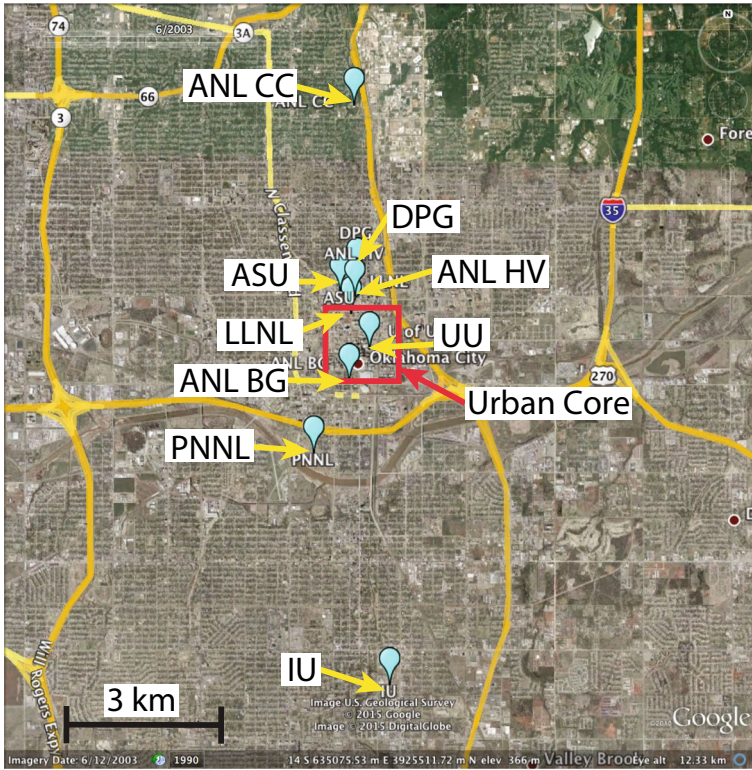


Fig. 1 Map of the subset of instruments deployed in and around Oklahoma City during Joint Urban 2003 that are used in this work. Instrument sites are indicated by yellow arrows and the urban core is indicated by the red box. The satellite image is courtesy of Google Earth, the U.S. Geological Survey, and DigitalGlobe

Table 1 JU2003 sodar instrument locations and characteristics

Organization	Label	Latitude (°)	Longitude (°)	Min/max height (m)	Resolution (m)
Pacific Northwest National Laboratory	PNNL	35.45295	-97.52534	30 / 500	10
Argonne National Laboratory	ANL BG	35.46474	-97.51822	15 / 200	5
University of Utah	UU	35.45295	-97.52534	38 / 218	5
Argonne National Laboratory	ANL HV	35.47866	-97.51707	15 / 165	5
Dugway Proving Ground	DPG	35.48203	-97.51668	5 / 200	5
Argonne National Laboratory	ANL CC	35.50999	-97.51726	15 / 200	5

Note that the rawinsondes were released from the PNNL sodar location. The Table is arranged by instrument located from south to north (nominally upwind to downwind)

Table 2 JU2003 sonic anemometer tower locations and characteristics

Organization	Label	Latitude (°)	Longitude (°)	Heights (m)
Indiana University	IU	35.41505	-97.51008	19.4, 37.3, 54.6, 79.6
Lawrence Livermore National Laboratory	LLNL	35.475718	-97.51784	7.8, 14.6, 21.5, 28.3, 42.5, 55.8, 69.7, 83.2

Table 3 Description of specific case studies from JU2003 IOPs

Case	IOP	Release	Day in July 2003	Start UTC (CDT)	Stop UTC (CDT)	120-m speed ($m s^{-1}$)	Prevailing direction (°)	Rapidly varying direction?
IOP2-R1	2	1	2	1600 (1100)	1800 (1300)	4.7–6.3	200–240	Yes
IOP2-R3	2	3	2	2000 (1500)	2200 (1700)	4.3–5.9	175–225	Yes
IOP6-R2	6	2	16	1600 (1100)	1800 (1300)	5.9–7.9	180–200	No
IOP8-R2	8	2	25	0600 (100)	0800 (300)	9.0–10.0	160–167	No

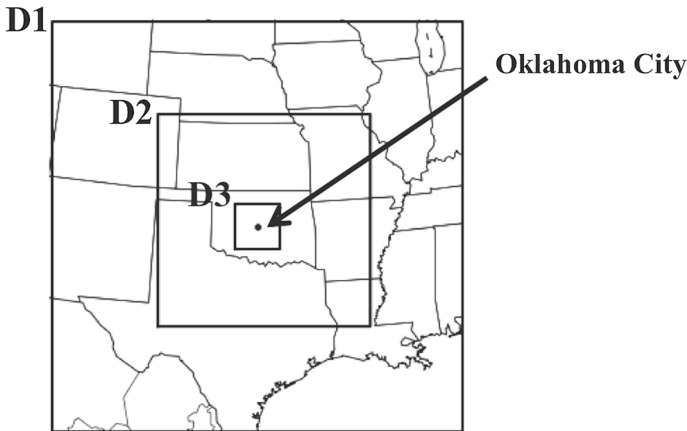


Fig. 2 A map of the WRF model domains used in this study and the location of Oklahoma City, where the Joint Urban 2003 campaign was conducted

3 WRF Model Simulations

The meteorological simulations were created using the Advanced Research WRF model (ARW) version 3.4.1. Figure 2 shows the three nested domains centred over Oklahoma City. The parameters for the three different WRF model simulations that were performed for these analyses are detailed in Table 4.

An examination of the literature reveals that all of the boundary-layer schemes that have been implemented in the WRF model have some biases (Lin et al. 2008; Hu et al. 2010;

Table 4 Simulation parameters for the three WRF model simulations used in these analyses

Basic	ZAM	UCM
Horizontal resolutions of 30, 10, and 3.3 km	All parameters from the Basic simulation with the following exception:	All parameters from the Basic simulation
37 vertical layers and the top of the model was set to 50 hPa	38 vertical layers and the top of the model was set to 50 hPa	Urban Canopy Model (UCM) (Kusaka and Kimura 2004)
Lowest model sigma levels: 1.000, 0.996, 0.990, 0.982, 0.974, 0.965, 0.955, 0.945, 0.932, 0.919, 0.904, 0.888, 0.870, 0.850, and 0.828	Lowest model sigma levels: 1.000, 0.999, 0.996, 0.990, 0.982, 0.974, 0.965, 0.955, 0.945, 0.932, 0.919, 0.904, 0.888, 0.870, 0.850, and 0.828	Uses a simplified urban geometry and includes:
Mellor-Yamada-Janjic (MYJ) boundary-layer physics scheme (Janjic 1994)	The lowest grid cell has a nominal centre at $z = 4$ m	Shadowing from buildings
Rapid radiative transfer model (RRTM) for long wave radiation (Mlawer et al. 1997)		Reflection of shortwave and longwave radiation
Dudhia shortwave radiation scheme (Dudhia 1989)		Canopy-layer wind profile
Eta similarity surface-layer physics		Multi-layer heat transfer equation for roof, wall and road surfaces
Noah land-surface scheme		
Thompson microphysics scheme (Thompson et al. 2008)		
Kain-Fritsch cumulus parametrization scheme (Kain 2004) was used only on the 30 and 10 km domains		

Xie et al. 2012). Even though the Mellor-Yamada-Janjic (MYJ) boundary-layer scheme uses local turbulence closure that may under estimate the vertical mixing under strongly unstable conditions (Hu et al. 2010; Xie et al. 2012), it was chosen due to its ability to directly export the TKE. The TKE is often used to determine the magnitude of turbulent mixing in many advanced plume dispersion modelling systems, including the one used in Part 2. The MYJ scheme is based on the Mellor-Yamada 2.5 boundary-layer scheme with modifications for NWP implementation made by Janjic (1994). Like other Reynolds-averaged Navier Stokes (RANS) turbulence closures, the MYJ scheme solves a prognostic equation for the ϵ and a diagnostic equation with a stability correction for the turbulent mixing length. This makes it possible to solve for the turbulent momentum diffusivity, which is then used to solve for the Reynolds shear stresses.

Initial and lateral boundary conditions were derived from the National Oceanic and Atmospheric Administration (NOAA) National Center for Environmental Prediction (NCEP) / National Center for Atmospheric Research (NCAR) Reanalysis Product (NNRP) (Kalnay et al. 2004). We use the PrepBuf observations that are provided by NOAA NCEP and are composed of a global set of surface and upper air reports operationally collected by the National Centers for Environmental Prediction (Keyser 2013). The observations include land surface, marine surface, radiosonde, pibal and aircraft reports from the Global Telecommunications System, profiler and US radar-derived winds, Special Sensor Microwave Image (SSM/I) oceanic winds and total column water retrievals, and satellite wind data from the National Environmental Satellite Data and Information Service. The information available in this dataset includes pressure, geopotential height, temperature, dew-point temperature, wind direction, and wind speed. The entire month of July 2003 was included in the simulations presented herein.

4 Analysis and Discussion

In the sections below, we compare and contrast the WRF model simulations with sodar, sonic, and rawinsonde observations that were taken upwind, downwind, and within the urban core, but primarily above the urban canopy. In Sect. 4.1 we focus on how the WRF model was able to simulate the temporal variation of the mean wind over the 1-month period of the Joint Urban 2003 field experiment and the vertical and horizontal variation during the 2-h intensive operating periods. In Sect. 4.2, we assess how well the WRF model can reproduce the measured turbulence. Finally, the model-derived boundary-layer depth is compared to values derived from potential temperature (θ) profile observations in Sect. 4.3.

4.1 Mean Winds

Figure 3 compares the time series of mean wind direction and wind speed for the Basic WRF model simulation and the PNNL sodar measurements at 120 m a.g.l. for the entire month of July 2003. The PNNL sodar was located about 1 km south-west of the urban core (see Fig. 1), effectively upwind of the urban core for the majority of the JU2003 field campaign due to the predominance of southerly winds. The model-computed wind directions and speeds tracked the diurnal variation of the observations most of the time, with an average absolute difference in wind direction and wind speed of 35° and 1.9 m s^{-1} , respectively. The average difference in wind direction and wind speed are -3° and 0.04 m s^{-1} , respectively. On 10 July and 22-23 July, the WRF model accurately predicts several large deviations from the predominant southerly wind direction, which are due to frontal passages. On 13 July and 19-

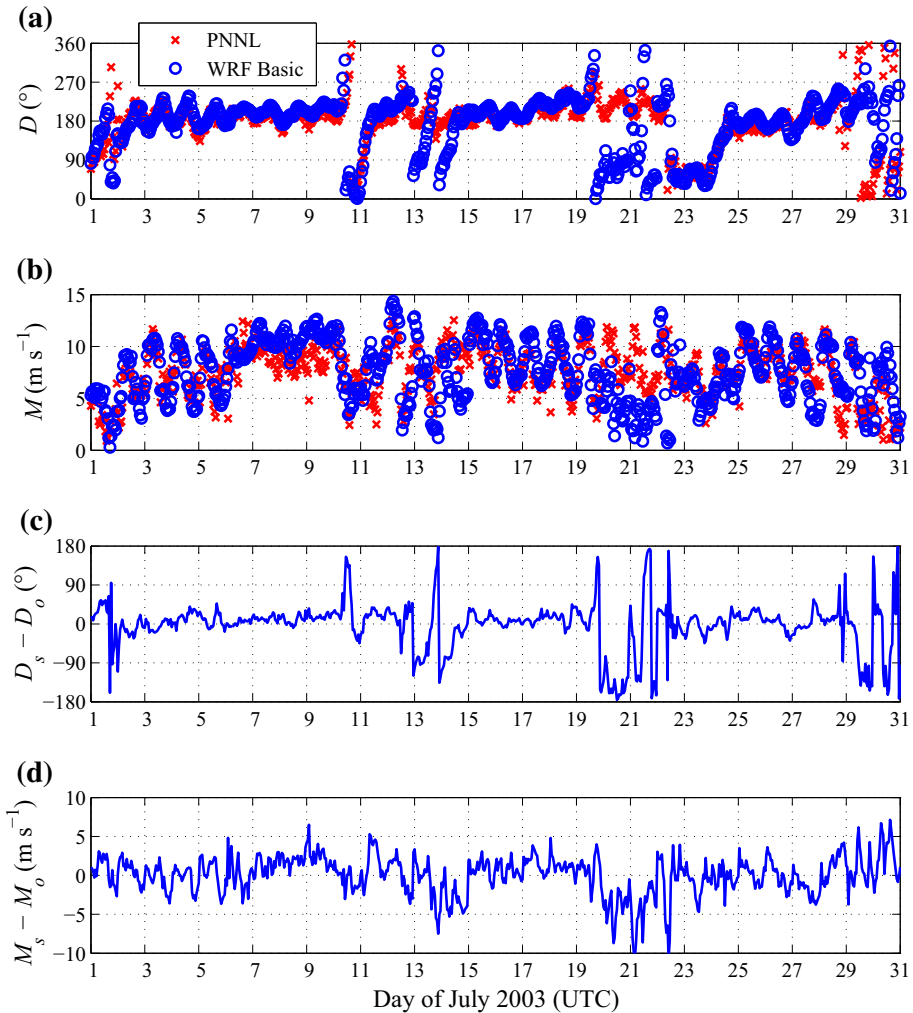


Fig. 3 Time series for the entire month of July 2003 showing a comparison of the **a** simulated and observed wind direction (D) and **b** the simulated and observed wind speed (M); and the difference between **c** the simulated (D_s) and observed (D_o) wind directions and **d** the simulated (M_s) and observed (M_o) wind speed. Observations are from the 120-m level of the PNNL sodar (using 1-h averages centred on the WRF model output time) and the 120-m level of the nearest cell-centred profile of the Basic WRF model simulation

21 July, however, the model simulations show 180° swings in the wind direction, while the observations do not. In general, the model-computed wind speeds track the measured values fairly well, but there are multi-hour or multi-day periods in which the model has significantly overestimated or underestimated the wind speed.

Figure 4 shows the histogram of the difference between the observed and predicted wind directions and wind speeds from Fig. 3. The WRF-computed wind directions are within $\pm 15^\circ$ of the measurements about 44 % of the time, between 15° and 30° 26 % of the time, between 30° and 45° 8 % of the time, and greater than 45° approximately 22 % of the time. The WRF-computed wind speeds are within $\pm 1 \text{ m s}^{-1}$ of the measurements about 36 % of the

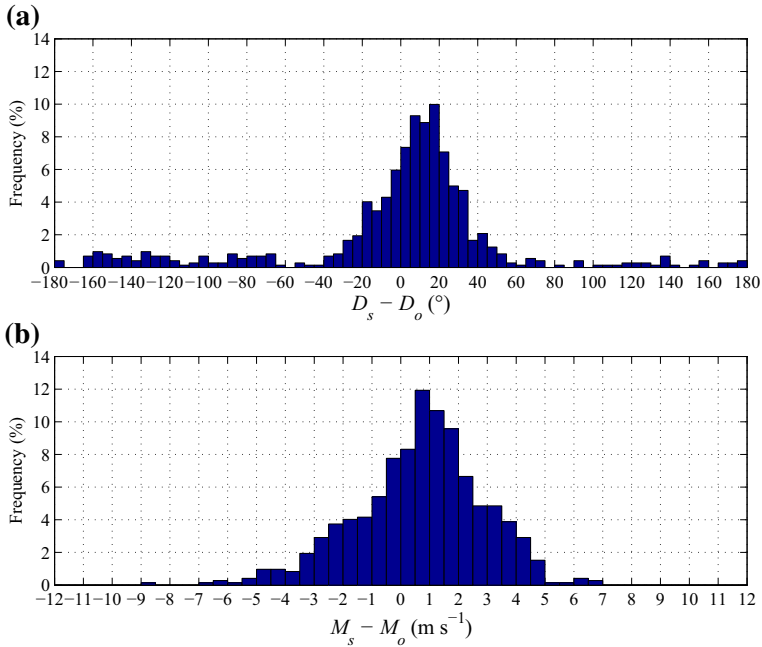


Fig. 4 Histogram of the absolute difference between the simulated and observed (*top*) wind direction and (*bottom*) speed for the entire month of July 2003 (a total of 721 data points). Observations are from the 120-m level of the PNNL sodar (using 1-h averages centred on the WRF model output time) and the 120-m level of the nearest cell-centred profile of the Basic WRF model simulation

time, between 1 and 2 m s⁻¹ 27 % of the time, between 2 and 3 m s⁻¹ 17 % of the time, and greater than 3 m s⁻¹ approximately 19 % of the time.

In Fig. 5, the wind speed and wind direction time series from the PNNL sodar at 120 m a.g.l. for IOPs 2, 6, and 8 are compared over an 8-h period with all three of the WRF model simulations (Basic, Z4M, and UCM as described in Table 4). The three WRF model simulations exhibit very similar behaviour, indicating that the WRF model simulations were not sensitive to the different near-surface options at the 120-m level. In general, the mesoscale model winds were smoothly varying in time, while the sodar observations showed high-frequency (compared to mesoscale) variation or meander on the sub-hourly scale. During IOP2, the WRF-computed wind speed matched the observations well during the first four hours, but then underestimated them by 1 to 3 m s⁻¹ in the latter 4 h. The model-computed wind direction, on the other hand, was off from 20° to 40° during the first two hours, but then captured some of the variation in the middle and latter parts of the IOP. The trend in the wind direction was captured in IOP6, but was almost exclusively clockwise from observations. The wind speed was correctly estimated, except for the first couple of hours. During IOP8, the wind speed was slightly overestimated for the entire period, while the model-computed wind direction diverged from the measurements over the 8-h period and was rotated consistently clockwise from the observations. Part 2 will investigate the effects of these deviations in wind speed and wind direction on the accuracy of point-to-point comparisons of simulated and observed plume statistics.

Figure 6 compares the wind vectors for IOP2-R1, as measured by the sodars with the Basic WRF model simulation at approximately 20, 60, 120, and 185 m a.g.l. (the approximate

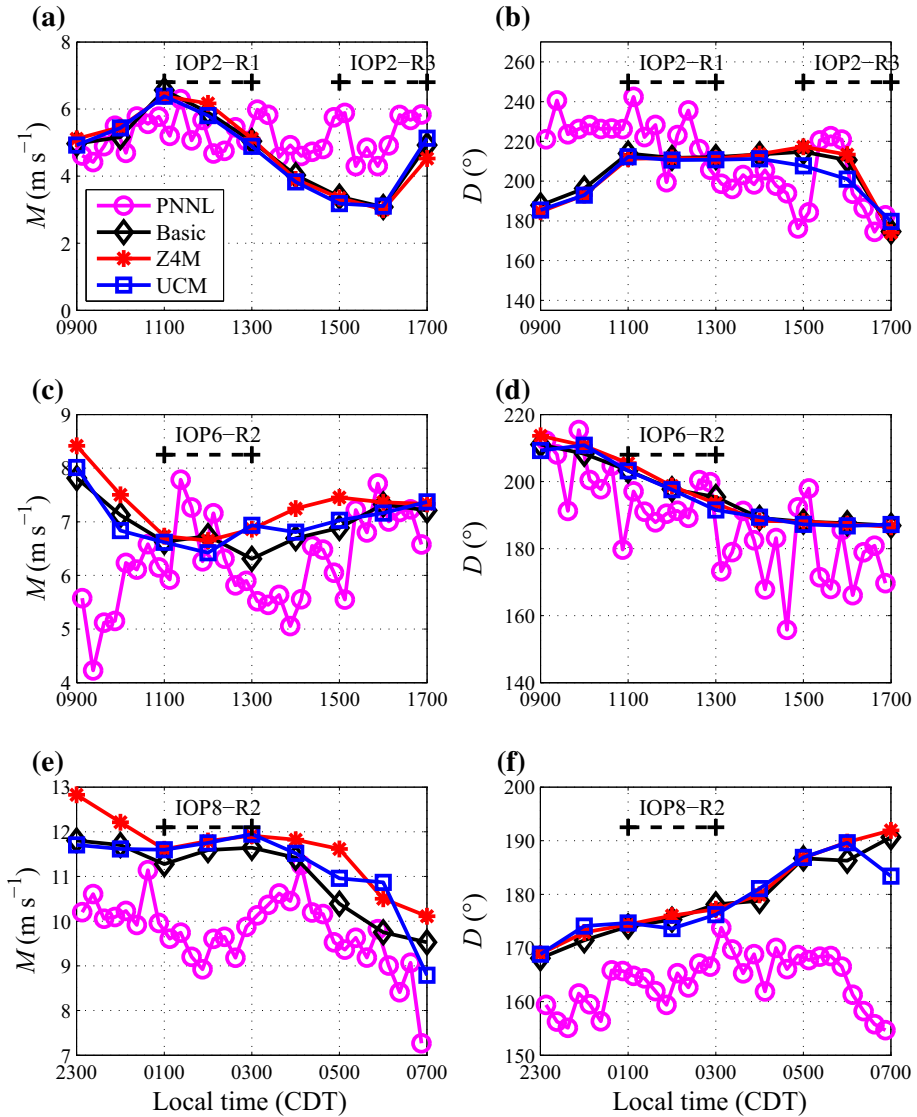


Fig. 5 The wind speed (a, c, e) and wind direction (b, d, f) time series for the entire duration of IOP2 (a, b), IOP6 (c, d), and IOP8 (e, f) as measured by the 120-m level of the PNNL sodar and the three WRF model simulations (Basic, Z4M, and UCM) described in Table 4

heights of the centres of the WRF model grid cells). The vectors for IOP2-R3, IOP6-R2, and IOP8-R2 are not shown because the only significant difference between those time periods and IOP2-R1 is found in the wind direction. As was seen in Fig. 5, all three WRF model simulations produce very similar velocity fields and therefore only the Basic WRF simulations are shown in Fig. 6. As one would expect in a region without significant topographical features, the sodar observations show uniform wind flow patterns around the urban core of Oklahoma City. The WRF model simulations are generally able to replicate the characteristics

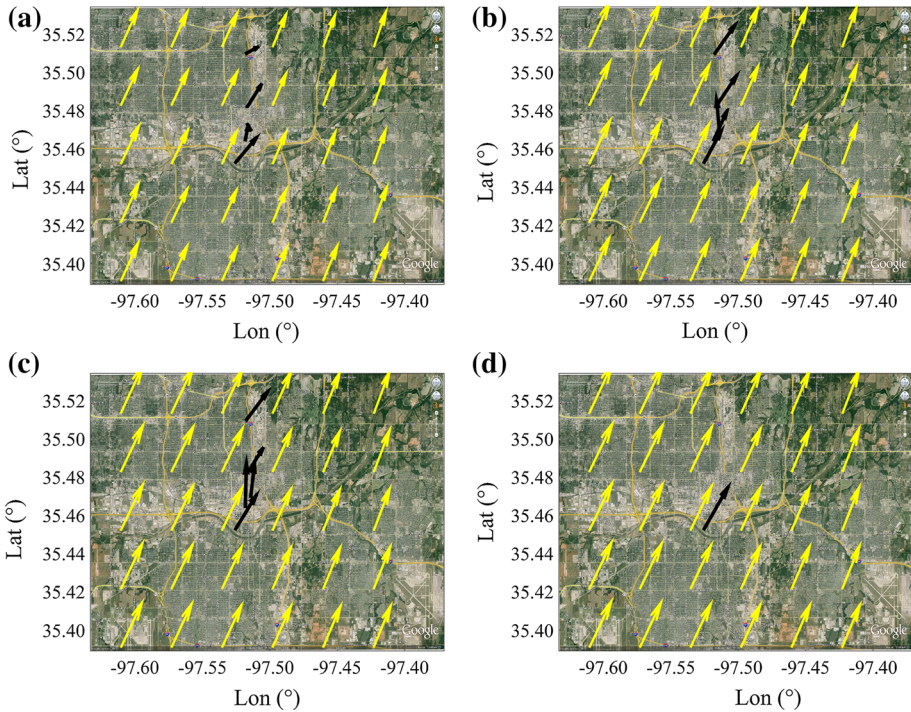


Fig. 6 Surface-layer mean wind velocity vectors from the Basic WRF model simulation (yellow) compared with JU2003 sodar data (black) from the first hour of IOP2-R1 (02 July 2003 1600 UTC (1100 CDT)) at four different heights. The satellite image is courtesy of Google Earth and the USDA Farm Service Agency

of the wind field measured in the surface layer during JU2003, but there is a noticeable error in the predicted wind direction. The error of 10 to 30° in the predicted wind direction over the course of the hour (see period from 1100 to 1200 in Fig. 5b) is similar to the errors in wind direction that have been observed by other studies that have used sub-kilometre horizontal resolutions (Tewari et al. 2010; Wyszogrodzki et al. 2012).

Figure 7 compares vertical profiles of wind speed and direction measured by three sodars (PNNL, ANL BG, and UU) during IOP2-R1 on 2 July 2003 between 1600 to 1700 UTC (1100 to 1200 CDT) compared with the three different WRF model simulations: Basic, Z4M, and UCM (see Table 4). The sodars are nominally aligned with the predominant southwesterly winds and located directly upwind of, within, and directly downwind of the urban core of Oklahoma City. The model-computed wind-speed profiles match the measurements of the PNNL sodar in Fig. 7a remarkably well. The model-computed wind direction is more southerly by 10 to 20° as compared to the 1-h measurements, but there is considerable scatter in the 15-min measurements (Fig. 7b). As the flow approaches the urban core, the increased surface roughness retards the near-surface flow as is seen in the profile measured by the ANL BG sodar in Fig. 7c, which is just upwind of the tallest buildings in the urban core. The WRF model simulations, including the one that employs the UCM option, overestimate the wind speed near the ground and are unable to accurately reproduce the drag effect of the buildings in the suburban, industrial and commercial zones upwind of the urban core. On the other hand, the 1-h wind direction measurements have rotated roughly 20° as compared to the ANL BG sodar measurements and now match the spatially invariant WRF-computed

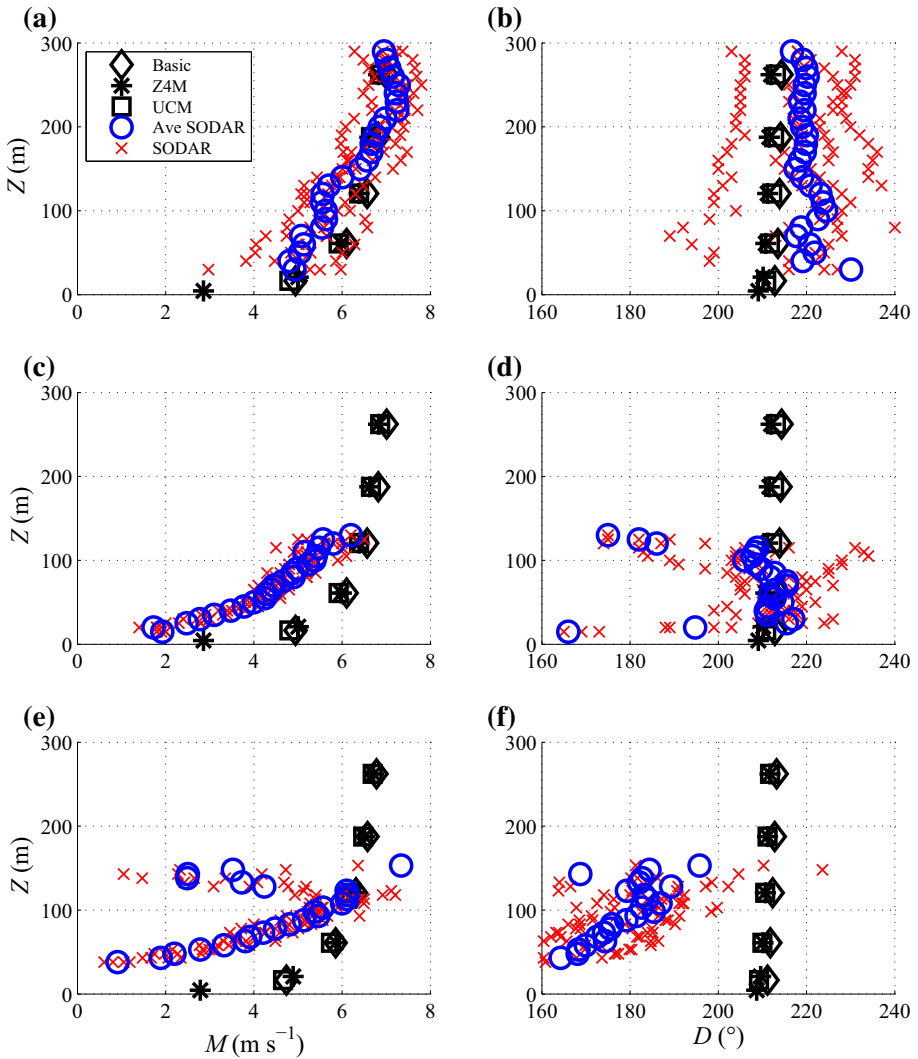


Fig. 7 Comparison of model-computed and measured vertical profiles of wind speed (a, c, e) and wind direction (b, d, f) for IOP2-R1 02 July 2003 between 1600 and 1700 UTC (1100 to 1200 CDT). Measurements are at the PNNL (a, b), ANL BG (c, d), and UU (e, f) sodars in order from upwind to immediately downwind of the urban core. *Red X's* indicate the individual 15-min profiles measured by the sodar and the *blue O's* are the 1-h average. The *black symbols* correspond to WRF model simulated fields at 1600 UTC for the three different simulations (Basic, Z4M, and UCM) detailed in Table 4

wind directions (Fig. 7d). At the UU sodar, located in the wake of the tall buildings in the urban core, the WRF model again overestimates the wind speed near the surface (Fig. 7e). The measured wind directions show significant variation with height and range from 160° to 185°, whereas the WRF model calculations are about 210° and constant with height (Fig. 7f). It appears that the effects of the buildings in the city centre have caused significant spatial (both horizontal and vertical) differences in the wind speed and wind direction that are not captured by the WRF model simulations.

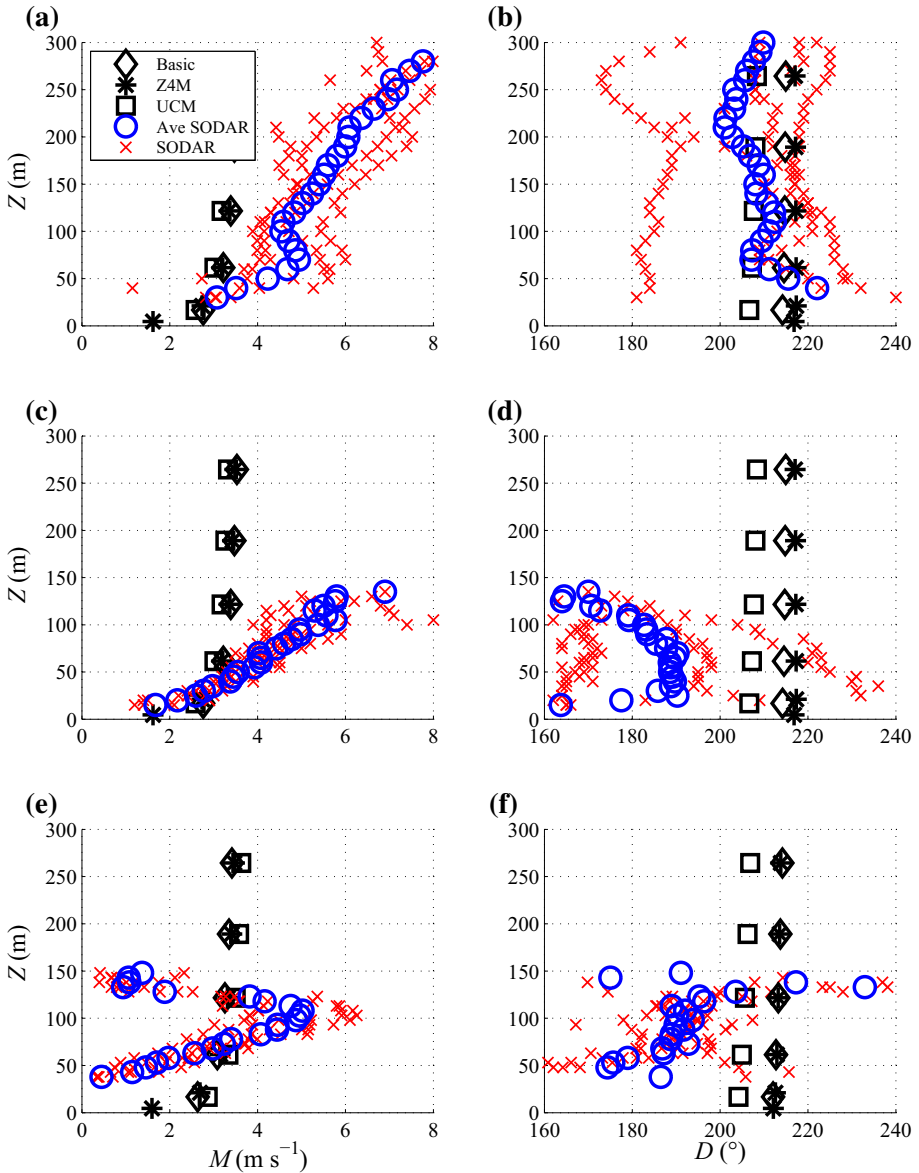


Fig. 8 Comparison of model-computed and measured vertical profiles of wind speed (a, c, e) and wind direction (b, d, f) for IOP2-R3 on 2 July 2003 between 2000 to 2100 UTC (1500 to 1600 CDT). Measurements are at the PNNL (a, b), ANL BG (c, d), and UU (e, f) sodars in order from upwind to immediately downwind of the urban core. *Red X's* indicate the individual 15-min profiles measured by the sodar and the *blue O's* are the 1-h average. The *black symbols* correspond to WRF model simulated fields at 2000 UTC for the three different simulations (Basic, Z4M, and UCM) detailed in Table 4

Figure 8 shows the vertical profiles of wind speed and wind direction measured by three sodars (PNNL, ANL BG, and UU) that are nominally in line with the predominant south-westerly winds during IOP2-R3 (2 July 2003 between 2000 to 2100 UTC (1500 to 1600 CDT))

compared with the three different WRF model simulations. The WRF model significantly underestimates the wind speed at the upwind PNNL location (Fig. 8a). The WRF-computed wind speeds decrease by nearly half as compared to four hours earlier (see Figs. 7a and 5a), whereas the sodar measurements show comparable wind speeds over this time period (see Figs 7a and 8a). The variation of wind speed with height is not well-captured by the WRF model for the in-city ANL BG and UU sodar locations. Similar to IOP2-R1 (Fig. 7), the model-computed wind directions do not change significantly from location to location, but the sodar measurements show significant differences (Fig. 8). Note that there is a large difference between the 15-min average (red crosses) and the 1-h average wind direction (blue circles) measured by the PNNL sodar during IOP2-R3 (Fig. 8b), which is due to the wind direction shifting from southerly winds to south-westerly winds over the course of the hour (see also Fig. 5b).

Figure 9 compares the vertical profiles of wind speed and wind direction measured by three sodars (PNNL, ANL BG, and UU) that are nominally aligned with the predominant south-westerly winds for IOP6-R2 (16 July 2003 between 2000 to 2100 UTC (1500 to 1600 CDT)) compared with the three different WRF model simulations. The WRF model was able to reproduce the observed upwind wind-speed profile quite well (see Fig. 9a), but similar to IOP2-R1 and IOP2-R3, the WRF model was unable to reproduce the retarded near-surface (below 100 m) wind speeds due to the presence of the large buildings just upwind of the urban core at the ANL BG sodar (Fig. 9c) and in the wake of the urban core at the UU sodar (Fig. 9e). Note that the sodar observations often exhibit a great deal of variability near the lower (e.g., Fig. 9a) and upper extent of their range, thus it is unclear whether the scatter seen below 70 m in the PNNL observations real or is simply a result of the limitations of the instrument at the extremes of its range. The difference between the model-computed and measured wind direction at the upwind PNNL sodar location was only 10° to 15° . However, as for the IOP2 cases, the wind direction in the urban core at the ANL BG and UU sodar locations was not well captured.

Figure 10 shows vertical profiles of the wind speed and wind direction measured by the three sodars (PNNL, ANL BG, and ANL HV) that were nominally aligned with the predominant south-south-easterly winds as the wind passes from 1.7 km upwind of, over, and 800 m downwind of the urban core of Oklahoma City during IOP8-R2 (25 July 2003 between 0600 to 0700 UTC (0100 to 0200 CDT)) and compares them with the three different WRF model simulations. The WRF model-computed profiles show reasonably good agreement with the profile measured by the upwind PNNL sodar in Figs. 10a, b although the simulated wind speeds are slightly overestimated. The shape of the wind-speed profiles exhibit the strong velocity gradients that are indicative of the effects of thermally stable conditions. As was the case with the profiles measured by the ANL BG sodar during the day in Figs. 7b, 8b, and 9b, the proximity of the buildings is also evident in the nighttime profile measurements in Fig. 10b. The WRF model calculations significantly overestimate the velocity at the ANL BG sodar site and the model-computed wind directions are off from 20° to 40° . The wake of the urban core is still evident in the reduction of mean wind speeds observed by the downwind ANL HV sodar (Fig. 10e) when compared to those observed by the upwind PNNL sodar in (Fig. 10a), even though the ANL HV sodar is nearly 1 km downwind of the large buildings in the urban core.

It should be noted that the mean wind speed measured by the sonic towers show similar trends relative to the WRF model simulations (regarding over- and/or underprediction of wind speed) that have been presented in the comparisons with sodar data above. However, as they do not provide any additional insight into the observed phenomena they have not been presented here.

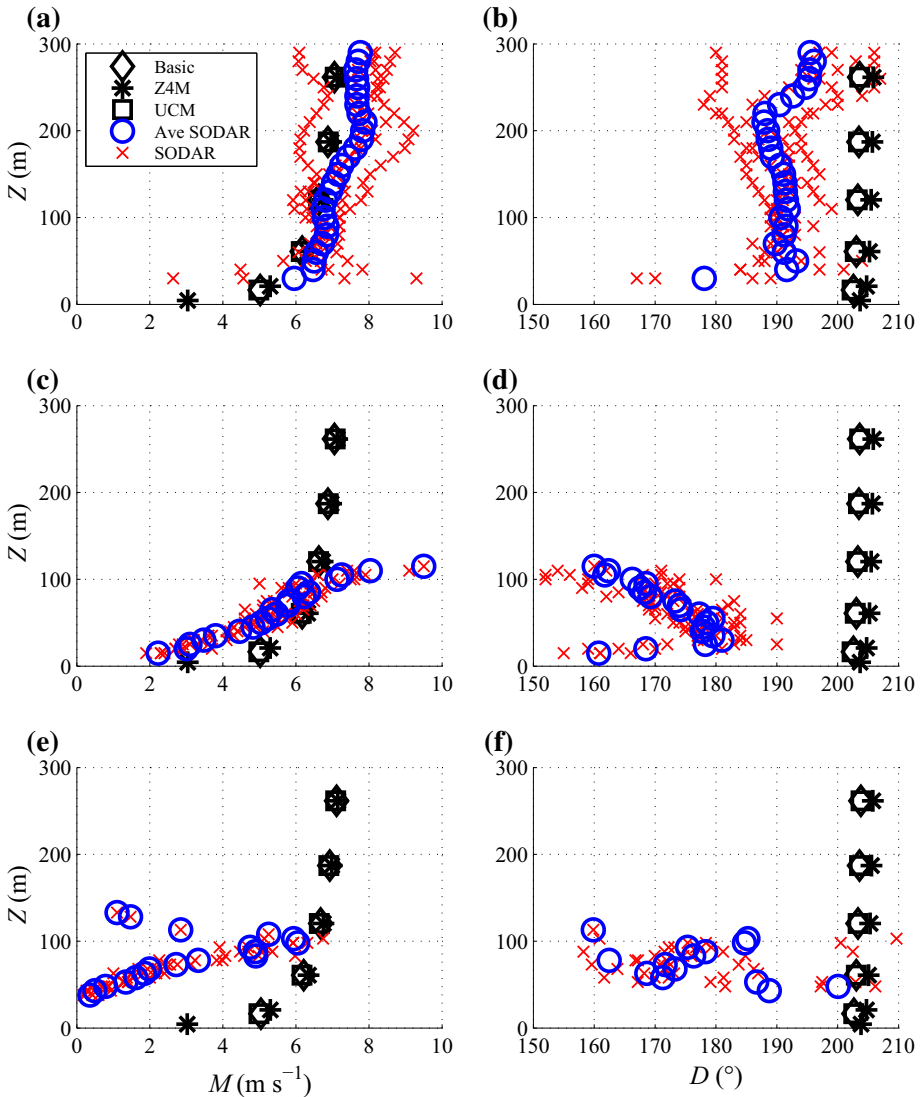


Fig. 9 Comparison of model-computed and measured vertical profiles of wind speed (a, c, e) and wind direction (b, d, f) for IOP6-R2 on 16 July 2003 between 1600 and 1700 UTC (1100 to 1200 CDT). Measurements are at the PNNL (a, b), ANL BG (c, d), and UU (e, f) sodars in order from upwind to immediately downwind of the urban core. Red X's indicate the individual 15-min profiles measured by the sodar and the blue O's are the 1-h average. The black symbols correspond to WRF model simulated fields at 1600 UTC for the three different simulations (Basic, Z4m, and UCM) detailed in Table 4

4.2 Turbulence

A month-long time series during July 2003 of measured versus model-computed e , u_* , and $1/L$ is given in Fig. 11. The measurements were obtained at the 55-m level of the IU sonic tower and compared with the corresponding quantities produced by the Basic WRF model

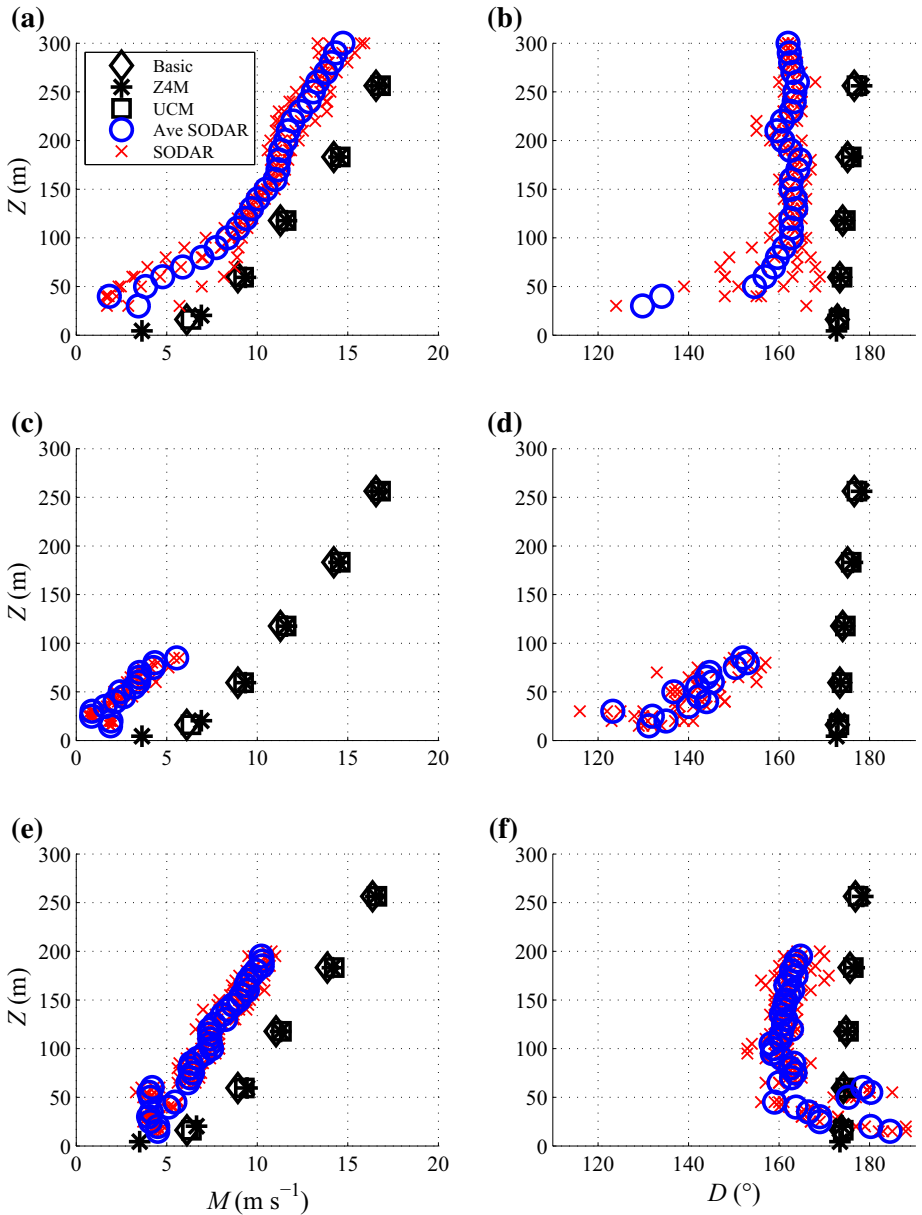


Fig. 10 Comparison of model-computed and measured vertical profiles of wind speed (a, c, e) and wind direction (b, d, f) for IOP8-R2 on 25 July 2003 between 0600 and 0700 UTC (0100 to 0200 CDT). Measurements are at the PNNL (a, b), ANL BG (c, d), and ANL HV (e, f) sodars in order from upwind to downwind of the urban core. Red X's indicate the individual 15-min profiles measured by the sodar and the blue O's are the 1-h average. The black symbols correspond to WRF model simulated fields at 0600 UTC for the three different simulations (Basic, Z4m, and UCM) detailed in Table 4

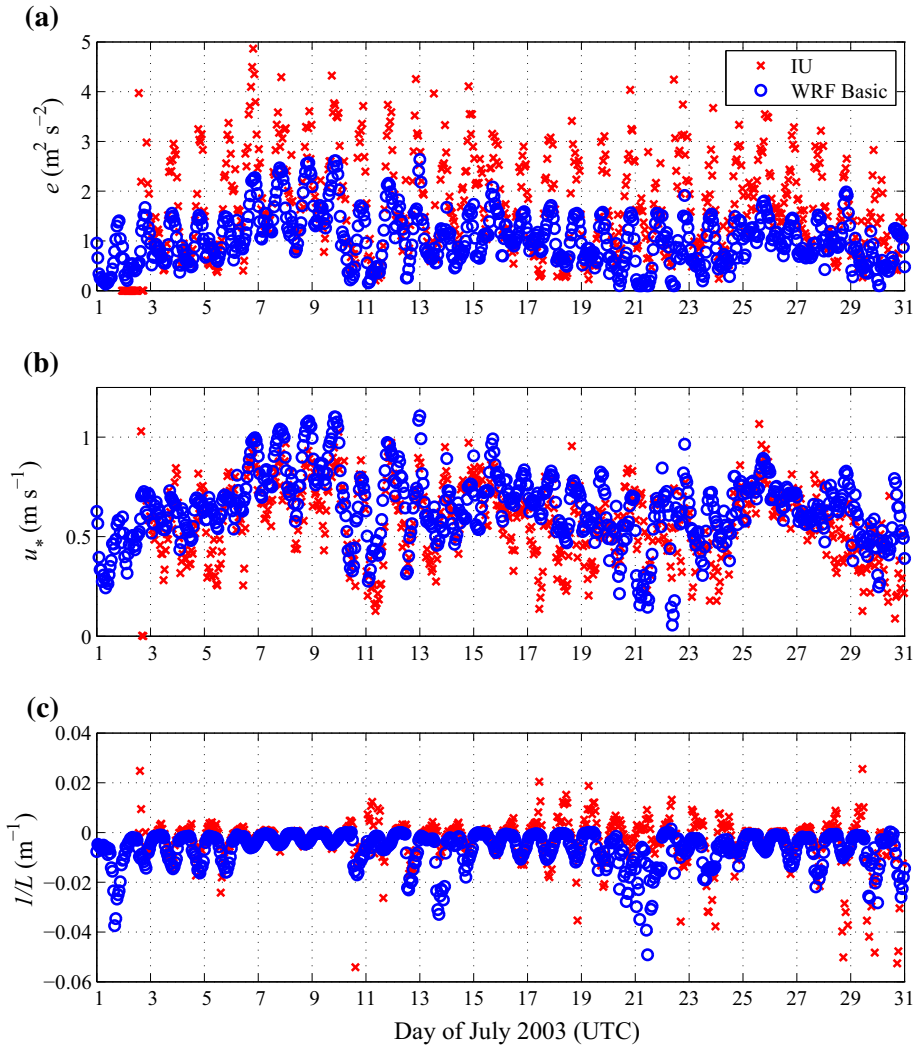


Fig. 11 Time series for the entire month of July 2003 showing a comparison of **a** the turbulent kinetic energy (e), **b** friction velocity (u_*), and **c** reciprocal Obukhov length ($1/L$) as observed by the 55-m level of the IU sonic tower (using 1-h averages) and the 60-m level of the Basic WRF model simulation

simulation. Note that the IU sonics were not operational on the first day of the month and part of the second day. The time series plot shows that the TKE computed by the WRF model consistently underpredicted the observations made during daytime hours, and at night underestimated TKE most of the time but occasionally overestimated the TKE (Fig. 11a). The daytime trend is consistent with the fact that the MYJ surface-layer scheme uses local closure (Hu et al. 2010; Xie et al. 2012), however the nighttime tendency is more surprising as this is when one would expect a local closure to perform well. The u_* values predicted by the WRF model exhibit a small overprediction bias, especially during nighttime hours (Fig. 11b). The WRF model had difficulty predicting $1/L$ (Fig. 11c) for the time periods when the WRF model was unable to properly predict the observed wind direction (see Fig. 3a). Moreover, the

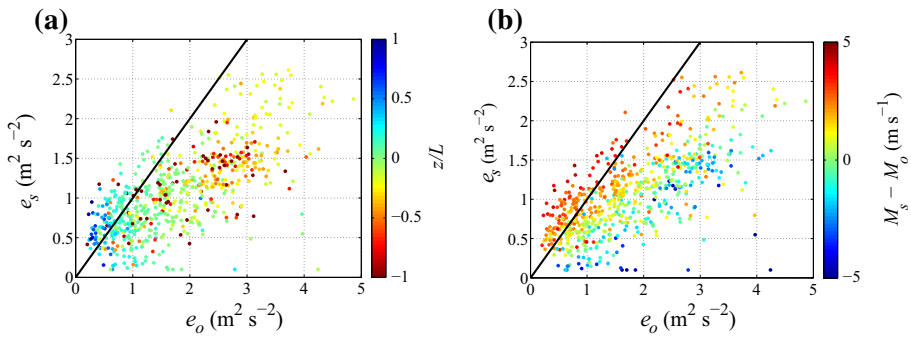


Fig. 12 Scatter plots of the observed and simulated turbulent kinetic energy (e_o and e_s , respectively) coloured by **a** the observed Monin–Obukhov stability parameter (z/L) and **b** the difference between the simulated and observed wind speeds ($M_s - M_o$). The one-to-one line is shown in black

WRF model predicts near-neutral stability ($1/L \approx 0$) during the nocturnal hours rather than the observed thermally stable conditions ($1/L > 0$). The behaviour of the model-computed $1/L$ may be in part due to the urban parametrizations within the WRF model since the IU sonic tower was located in a suburban area.

Since the e typically scales with wind speed and is enhanced under unstable conditions and suppressed under stable conditions, the time series of the observed and simulated turbulent kinetic energy (e_o and e_s , respectively) in Fig. 11a are put in scatter plot form and the symbols coloured by the measured stability and the model computed and measured wind speed difference (Fig. 12). Figure 12a colours the data by the locally-measured Monin–Obukhov stability parameter (z/L), which reveals that TKE was typically underpredicted by the WRF model during unstable conditions ($z/L < 0$), and slightly overpredicted during stronger stable conditions ($z/L > 0.5$). The WRF model overprediction during stable conditions is likely due to the neutral conditions computed by the WRF model during the nighttime hours (see Fig. 11c). Figure 12b colours the data by the wind-speed difference ($M_s - M_o$) and shows that: a) the WRF model overprediction of TKE is nearly always correlated with a large overprediction of the mean wind speed; b) when the WRF-model-computed TKE matches the measurements, the wind speed is typically overpredicted by the WRF model; c) accurate prediction of the wind speed almost uniformly leads to an underprediction of TKE; and d) an underprediction of wind speed leads to an even greater underprediction in TKE. The results here suggest that the daytime underprediction of TKE cannot be simply explained by the WRF model underestimating the wind speed. Since the model underprediction of TKE is correlated with unstable conditions ($z/L < 0$), it could be partially due to known deficiencies in gradient-based turbulence closures in capturing the non-local mixing that occurs in convective conditions (e.g., Stull 1988; Hu et al. 2010; Xie et al. 2012).

Vertical profiles of e measured at the IU and LLNL sonic towers located in upwind suburban and downwind wake zones, respectively, are compared to the WRF model-computed profiles for several of the intensive operating periods in Fig. 13. Unfortunately, the IU sonics were not operational during IOP2-R1. Figures 13a and b show the observed and model-computed TKE profiles for IOP2-R3 at the IU and LLNL sonic towers, respectively. The WRF model underpredicts the maximum measured TKE by a factor of approximately 1.5 to 1.6. This underprediction might be explained by the fact that all three WRF model simulations predicted a significantly slower upper-level wind speed than was observed during this time period, (see Figs. 5a, 8), which would naturally lead to an underprediction of the turbulence.

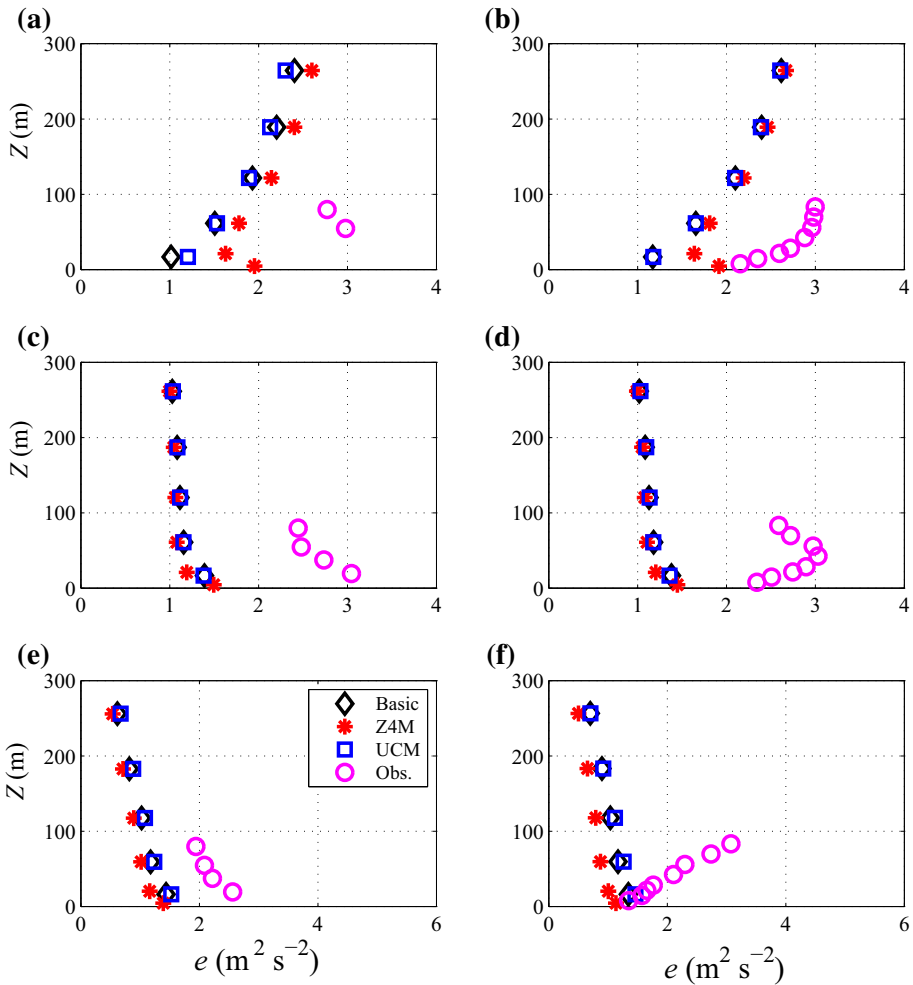


Fig. 13 Measured and model-computed TKE profiles (*magenta and black symbols, respectively*) at the IU (a, c, e) and LLNL (b, d, f) sonic towers from a, b IOP2-R3, 2 July 2003 between 2000 and 2100 UTC (1500 to 1600 CDT), c, d IOP6-R2, 16 July 2003 between 1600 and 1700 UTC (1100 to 1200 CDT), and e, f IOP8-R2, 25 July 2003 between 0600 and 0700 UTC (0100 to 0200 CDT)

The measured TKE in the wake of the urban core (Fig. 13b) is only slightly larger than the suburban values at the same height (Fig. 13a). Although there are several buildings that are at least 100-m tall in the urban core (Burian et al. 2003), none of them are directly upwind of the LLNL tower location due to the south-westerly prevailing winds at this time. There is an 88-m tall building about 250 m to the south-south-east of the LLNL tower, which would have been upwind of the tower for at least some of the hour in question due to the shifting wind direction (see Fig. 5b). It is also noteworthy that the TKE observations at the IU tower do not increase with height at the two active levels as one would normally expect under thermally unstable conditions (and as is predicted by the WRF model simulations for IOP2-R3). An examination of the hourly TKE profiles from the IU tower over the course of the entire JU2003 field campaign (not shown) indicated that while there were instances where the observations

exhibited the increasing TKE with height that is typical of the lower portion of a thermally unstable boundary layer, TKE observations of the IU tower would more commonly decrease with height as one might associate with a thermally neutral or stable boundary layer. This behaviour is likely due to the mechanical mixing within the suburban canopy, which will generate additional turbulence at the top of the canopy.

The daytime TKE profiles during IOP6-R2 from the IU and LLNL sonic towers are shown in Figs. 13c and d. Interestingly, the modelled and observed TKE profiles resemble the thermally stable profiles shown in Fig. 13e rather than the profile that is characteristic of thermally unstable conditions in Fig. 13a in spite of being acquired late in the morning. As will be shown in the following section, IOP6-R2 (late morning) had a much lower boundary-layer height than was observed during IOP2-R3 (late afternoon) and as such the TKE profile is exhibiting more thermally neutral behaviour. The sonics near the urban core on the LLNL tower exhibit very similar behaviour to what was observed during IOP2-R3 in Fig. 13b.

The nighttime TKE profiles during IOP8-R2 from the IU and LLNL sonic towers are shown in Figs. 13e and f. Both the WRF model computed and measured TKE at the upwind IU sonic exhibit the typical nighttime characteristic of TKE decaying with height, although the WRF model underestimates the measured values by about a factor of 2. The wind speed from the WRF model simulation for this case fairly accurately reproduces the measured winds upwind of the city center (see Figs. 5c, 10a), so the model underestimation of the measured TKE cannot be linked to an underestimation of the modelled wind speed. The WRF model accurately predicted the Obukhov stability parameter this night (see Fig. 11c), therefore differences in atmospheric stratification are not likely the cause either. Figure 13f clearly shows the effects of the urban terrain on the turbulence measured by the LLNL sonics as e increases to $6 \text{ m}^2 \text{ s}^{-2}$, double that found in the other IOPs. The height of the measured maximum TKE is nearly the same height as the 88-m tall building that is upwind of the LLNL tower for the prevailing south-south-easterly wind (see Fig. 5c). It is, of course, not possible for the WRF model to capture individual building effects given its relatively coarse horizontal grid resolution.

There are many different factors that affect the turbulence that is predicted in the WRF-model, which combine to cause the distinct bias in the WRF-model computed TKE. The factors that will most obviously affect TKE are the predicted wind speed, velocity gradients, and thermal stability. As was discussed above, Fig. 11d clearly shows that the WRF model underpredicts the observed TKE in nearly all circumstances and that the underpredicted TKE is not due to any bias in the predicted wind speed. As was previously discussed and shown in Fig. 4b there was a slight bias toward the WRF model overpredicting the wind speed, which should act to increase the predicted TKE. A bias toward the WRF model predicting more unstable conditions than was observed is shown in Fig. 11b, which should also act to increase the predicted TKE. A histogram of the difference between the predicted and observed wind speeds from the 60-m level of the PNNL sodar (not shown) had a similar bias toward overpredicting the wind speed as was observed with the 120-m sodar observations in Fig. 4b. The 60-m histogram had a difference of 0.66 m s^{-1} on average and an absolute average difference of 1.8 m s^{-1} . The fact that the 120-m average difference is less than the 60-m average difference indicates the velocity gradients are underpredicted on average. Since the predicted turbulence is directly proportional to the velocity gradient, this would act to reduce the predicted turbulence thus contributing to the observed underprediction of TKE. One would normally associate an underestimation in near-surface velocity gradients with an underestimation in u_* , which was shown in Fig. 11b to be consistently overestimated. However, as 60 m and 120 m are the centres of the second and third cells above the ground in the WRF model simulations (except for the Z4M simulation that has an additional near-

surface cell) this is indicative of the WRF model concentrating more of the transition from the no-slip condition at the surface to the flow at the top of the boundary layer in the first grid cell. Additionally, the magnitude of TKE is sensitive to the turbulent-length-scale formulation that is known to contain considerable uncertainty (e.g., Cuxart et al. 2006). It is beyond the scope of this paper, however, to estimate the turbulent mixing length from the tower sonic measurements, and thus we cannot say with certainty why the WRF model is underpredicting TKE.

4.3 Boundary-Layer Height

There are a variety of methods that are commonly used to estimate h both within mesoscale models (e.g., Liu et al. 2006) and in experimental data (e.g., Liu and Liang 2010; Stull 1988). Unfortunately the different methods tend to produce significantly different estimates of h depending on which parameters and/or profile features are used in the estimate. The definition of h varies with the thermal stability conditions. Under thermally unstable and neutral conditions it is often defined as the base of the inversion layer that separates the boundary-layer flow from the free atmosphere. Under thermally-stable conditions it is often defined as the top of the surface inversion layer (Liu and Liang 2010) or the height at which the TKE reaches 10% of its maximum value (Brown 2001).

Figure 14 shows the θ and water-vapour mixing ratio (Q_{vapor}) profiles, respectively, as measured by the PNNL rawinsonde and simulated fields from all three WRF model simulations on (a, b) 2 July 2003 at 2000 UTC (1500 CDT), (c, d) 16 July 2003 at 1600 UTC (1100 CDT), and (e, f) 25 July 2003 at 0600 UTC (0100 CDT). The observed h shown in Fig. 14 is calculated based on the height at which the θ gradient reaches at least 0.004 K m^{-1} (Liu and Liang 2010). The WRF model uses a simple definition for h as being the height above the surface where TKE decreases to a value of $0.1 \text{ m}^2 \text{ s}^{-2}$. Note that the TKE-threshold method employed by the WRF models MYJ scheme not only overestimates the h derived from the simulated θ profiles, but also the h derived from the observed θ profile.

The strong thermally unstable conditions present during the late afternoon in IOP2-R3 (2000 UTC, 1500 CDT) shown in Figs. 14a and b) have produced a very deep boundary layer. The MYJ surface-layer scheme's method of calculating h estimates values of at least 3.5 km (for the Basic simulation, the other simulations predict still higher values of nearly 4 km). Using the θ -gradient method with the rawinsonde observations produces a value of approximately 2 km. If the θ -gradient method was used instead of the TKE-threshold method that is currently employed in the MYJ boundary-layer scheme it would estimate h to be approximately 3 km.

The θ and Q_{vapor} profiles from the late morning during IOP6-R2 (16 July 2003 at 1600 UTC (1100 CDT)) in Figs. 14c, d show that the boundary layer has not yet fully developed and is more shallow than it was during IOP2-R3. In this case the Basic simulation provides the largest estimate of h at approximately 1000 m, while the other two WRF model simulations estimate h to be approximately 850 m. The θ -gradient method with the rawinsonde observations produces a value of approximately 780 m. The θ -gradient method applied to the WRF-calculated θ profiles would yield estimates of h just under 600 m.

The nocturnal θ and Q_{vapor} profiles at the PNNL rawinsonde measurement location are shown in Figs. 14e, f. The MYJ surface-layer scheme's method of calculating h again produces a significant overprediction when compared to using a h based on the θ profile. It should be noted that the θ profiles measured during IOP8-R2 have a shape more characteristic of neutral thermal stability (Liu and Liang 2010), which is not overly surprising given that it is measured deep within the suburbs of Oklahoma City. For this thermally-stable time period,

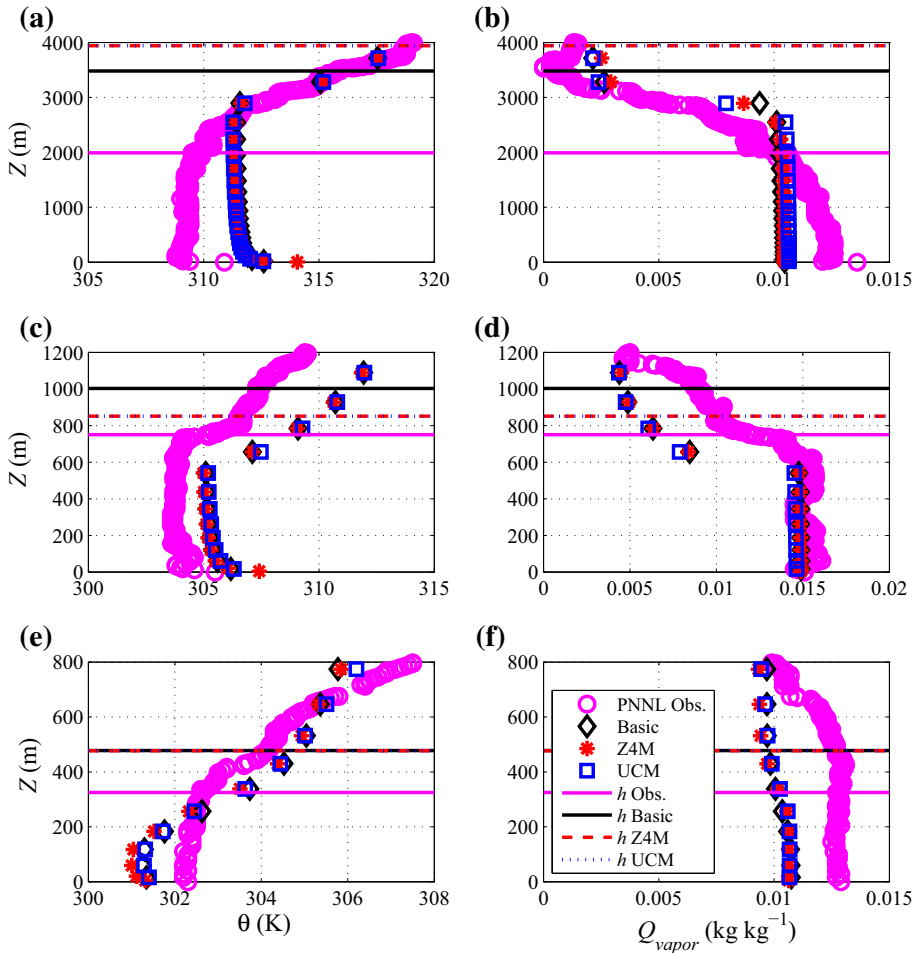


Fig. 14 Vertical profiles of observed and model-computed (a, c, e). Potential temperature and (b, d, f) water vapour mixing ratio for a, b the start of IOP2-R3, 2 July 2003 at 2000 UTC (1500 CDT), c, d the start of IOP6-R2 (16 July 2003 at 1600 UTC (1100 CDT)), and e, f the start of IOP8-R2 (25 July 2003 at 0600 UTC (0100 CDT)) compared with WRF-model simulated fields (black, red and blue symbols corresponding to the three simulations detailed in Table 4). The horizontal lines indicate the observed and WRF model-computed boundary-layer heights (line colours match the corresponding profile symbols)

the θ profile predicted by the WRF model would indicate an even smaller h than is seen in the measured θ profile (approximately 120 m and 340 m, respectively). Whereas each of the three WRF model simulations estimate h to be approximately 480 m. Q_{vapor} is underestimated in both IOP2-R3 (Fig. 13b) and IOP8-R2 (Fig. 13e) but are accurately predicted during IOP6-R2 (Fig. 14d). The underestimation of the amount of moisture in the air is what likely contributes to the WRF model simulations being overly sensitive to the influence of the diurnal cycle, i.e., overpredicting h during daytime hours and underpredicting it at night (using θ based h estimates instead of TKE).

Figure 14 indicates that during the daytime IOPs, the WRF-computed near-surface temperatures were higher than the measurements, while at night the WRF-computed surface temperature was lower. The former indicates the possibility of stronger influences of solar

heating of the surface in the WRF model simulation with resultant higher boundary-layer heights (using the θ profile rather than the TKE-threshold method that is currently employed by the WRF model's MYJ boundary-layer scheme) during the day and more cooling at night yielding lower boundary-layer heights at night than was observed in the JU2003 data. The sensitivity of the WRF model simulations used in these analyses to solar heating could be due to the WRF model predicting warmer and drier conditions than were observed. This is a trend that was opposite to the one that was observed in the WRF model simulations using MYJ by some previous studies (Hu et al. 2010; Xie et al. 2012). These trends may be due to errors in the NCEP/NCAR reanalysis data surface moisture and temperature initial conditions for the WRF model, which has been shown to lead to constant biases in simulations (Chen et al. 2007). However, the initial soil temperature and moisture were found to have reasonable values. July 2003 was an abnormally dry month for the region (the 15th driest on record). Both observations and simulations showed very little precipitation over the month. These unusually dry conditions may have lead to the overprediction of temperatures and the effects on the boundary-layer heights.

5 Conclusions

The WRF model was evaluated against meteorological data collected during the Joint Urban 2003 tracer field experiment conducted in Oklahoma City in July 2003. Measurements from a range of meteorological instrumentation including sodars, rawinsondes, and sonic towers were used to evaluate the temporal, horizontal and vertical variations of the wind, turbulence, and other parameters important to plume transport and dispersion models. The WRF model was run in three configurations: a basic mode, a higher near-surface vertical resolution mode, and an urban canopy parametrization mode.

An examination of the WRF model's ability to reproduce 120-m wind speed and direction over the month-long JU2003 experimental campaign in a suburban area to the south (and typically upwind) of the Oklahoma City central business district indicated that the model was able to reasonably account for the diurnal variation of the wind speed and wind direction, as well as account for several abrupt changes due to the passage of fronts. In a few instances, however, the predicted wind direction shifted considerably from the average while the observations remained fairly steady. The mean absolute wind-direction difference over the month-long period was found to be 35° , which is consistent with other studies that used significantly finer horizontal resolution (Tewari et al. 2010; Wyszogrodzki et al. 2012). Three 8-h intensive operating periods (IOP2, IOP6, and IOP8) were chosen to evaluate the vertical wind structure, as well as the temporal and horizontal wind variation. Although the WRF model predicted the 120-m wind speed well on average over the entire month at the southerly suburban site, it significantly underpredicted the wind speed in the latter half of IOP2 and significantly overpredicted during the first few hours of IOP6. The WRF model was able to reproduce the 120-m level wind direction within $\pm 15^\circ$ during the 2-h time periods examined here, though there were several periods when there was a 30° to 40° wind-direction error. Additionally, the WRF model simulations were not able to reproduce the observed wind meander that occurred at 1- and 2-h intervals. The WRF model also struggled with capturing the vertical variation of the wind speed and wind direction at locations within or just downwind of the urban core.

During the IOPs, the WRF model was found to underpredict e at both the upwind suburban location of the IU sonic tower and at the LLNL sonic tower in the wake of the urban core for

both the daytime and nighttime periods. A month-long examination of e measured at the IU sonic tower at the 55-m level revealed a consistent underprediction of the TKE during the daytime, and a bias towards overprediction during stable conditions. Different mechanisms for these differences were explored, but it was difficult to pinpoint the exact reason(s) behind this result.

The boundary-layer depth measured in the suburban area to the south of the central business district was typically overestimated by the WRF model during the intensive operating periods. We believe this is primarily due to the WRF model using a fixed threshold value of $e = 0.1 \text{ m}^2 \text{ s}^{-2}$ to determine h rather than gradients in the θ profile or the height at which e reaches a small percentage of the maximum value. The WRF model's TKE-threshold method predicted boundary-layer height values that were about 1.75 (day) and 1.5 (night) times larger than the θ -profile-gradient method applied to JU2003 data and 1.2 (day) and 2.6 (night) times the height of the θ -profile method applied to the WRF model data.

All three of the WRF model simulations produced very similar results regardless of whether the [Kusaka and Kimura \(2004\)](#) single-layer urban canopy model or increased vertical resolution at the ground were used. None of the three WRF model simulations was able to adequately account for the depletion of momentum from the mean velocity profile due to the enhanced drag resulting from buildings in the urban core. While no mesoscale model can be expected to account for the effects of individual buildings on flow, turbulence, and near-source atmospheric transport and dispersion in urban areas, it remains to be seen whether it is possible for mesoscale models to accurately simulate the bulk effects of large-scale urban roughness on the wind field and turbulence. A more sophisticated multi-layer urban canopy model (e.g., [Chin et al. 2005](#); [Chen et al. 2011](#); [Salamanca et al. 2011](#)) may be able to more accurately account for urban effects on the mean wind and turbulence profiles, and should be investigated in the future.

Acknowledgments The Joint Urban 2003 field campaign was supported by the Defense Threat Reduction Agency and Dugway Proving Ground through a contract with the H. E. Cramer Company, Inc. The authors also acknowledge the hard work of the other JU2003 team workers and others that contributed to the datasets and figures presented in this work. In addition, the authors are very grateful to the local government workers, business owners and workers, and citizens of Oklahoma City who made the JU2003 field experiment possible.

References

- Allwine KJ, Leach MJ, Stockham LW, Shinn JS, Hosker RP, Bowers JF, Pace JC (2004) Overview of Joint Urban 2003—an atmospheric dispersion study in Oklahoma City. In: Symposium on planning, nowcasting, and forecasting in the urban zone, American Meteorological Society, Seattle, p J7.1
- Arya SP (1999) Air pollution meteorology and dispersion, 1st edn. Oxford University Press, New York, 310 pp
- Brown MJ (2001) Urban parameterizations for mesoscale models. In: Boybeyi Z (ed) Mesoscale atmospheric dispersion. WIT Press, Southampton, pp 193–255
- Brown MJ, Boswell D, Streit G, Nelson M, McPherson T, Hilton T, Pardyjak ER, Pol S, Ramamurthy P, Hansen B, Kastner-Klein P, Clark J, Moore A, Felton N, Strickland D, Brook D, Princevac M, Zajic D, Wayson R, MacDonald J, Fleming G, Storwold D (2004) Joint Urban 2003 street canyon experiment. In: Symposium on planning, nowcasting, and forecasting in the urban zone, American Meteorological Society, Seattle., p J7.3
- Burian S, Han W, Brown M (2003) Morphological analyses using 3D building databases: Oklahoma City, Oklahoma. Technical Report LA-UR-05-1821, LANL, Los Alamos, NM, U.S.A
- Chen F, Manning KW, LeMone MA, Trier SB, Alfieri JG, Roberts R, Tewari M, Niyogi D, Horst TW, Oncely SP, Basara JB, Blanken PD (2007) Description and evaluation of the characteristics of the near high-resolution land data assimilation system. *J Appl Meteorol Clim* 46:694–713

- Chen F, Kusaka H, Bornstein R, Ching J, Grimmond CSB, Grossman-Clarke S, Loridan T, Manning KW, Martilli A, Miao S, Sailor D, Salamanca FP, Taha H, Tewari M, Wang X, WA A, Zhang C (2011) The integrated wrf/urban modeling system: development, evaluation, and applications to urban environmental problems. *Int J Climatol* 31:273–288
- Chin HNS, Leach MJ, Sugiyama GA, Leone JM Jr, Walker H, Nasstrom JS, Brown MJ (2005) Evaluation of an urban canopy parameterization in a mesoscale model using VTMX and URBAN 2000 data. *Mon Weather Rev* 133(7):2043–2068
- Cuxart J, Holtstlag AAM, Beare RJ, Bazile E, Beljaars A, Cheng A, Conangla L, Ek M, Freedman F, Hamdi R, Kerstein A, Kitagawa H, Lenderink G, Lewellen D, Mailhot J, Mauritsen T, Perov V, Schayes G, Steeneveld GJ, Svensson G, Taylor P, Weng W, Wunsch S, Xu KM (2006) Single-column model inter-comparison for a stably stratified atmospheric boundary layer. *Boundary-Layer Meteorol* 118:273–303
- Dudhia J (1989) Numerical study of convection observed during the winter monsoon experiment using a mesoscale two-dimensional model. *J Atmos Sci* 46:3077–3107
- Hu XM, Nielsen-Gammon JW, Fa Zhang (2010) Evaluation of three planetary boundary layer schemes in the wrf model. *J Appl Meteorol Clim* 49:1831–1844
- Janjic ZI (1994) The step-mountain eta coordinate model: further developments of the convection, viscous layer, and turbulence closure schemes. *Mon Weather Rev* 122:927–945
- Kain JS (2004) The kainfrisch convective parameterization: an update. *J Appl Meteorol* 43:170–181
- Kalnay E, Kanamitsu M, Kistler R, Collins W, Deaven D, Gandin L, Iredell M, Saha S, White G, Woollen J, Zhu Y, Chelliah M, Ebisuzaki W, Higgins W, Janowiak J, Mo KC, Ropelewski C, Wang J, Leetmaa A, Reynolds R, Jenne R, Joseph D (2004) The NCEP/NCAR 40-year reanalysis project. *Bull Am Meteorol Soc* 77:437–471
- Keyser D (2013) NOAA NCEP PrepBuf observation description. http://www.emc.ncep.noaa.gov/mmb/data_processing/prepbuf/doc/document.htm. Accessed 4 Apr 2015
- Kusaka H, Kimura F (2004) Coupling a single-layer urban canopy model with a simple atmospheric model: impact on urban heat island simulation for an idealized case. *J Meteor Soc Jpn* 82:67–80
- Lin CY, Chen F, Huang JC, Chen WC, Liou YA, Chen WN, Liu SC (2008) Urban heat island effect and its impact on boundary layer development and land sea circulation over northern Taiwan. *Atmos Environ* 42:5635–5649
- Liu S, Liang XZ (2010) Observed diurnal cycle climatology of planetary boundary layer height. *J Clim* 23:5790–5809
- Liu Y, Chen F, Warner T, Basara J (2006) Verification of a mesoscale data-assimilation and forecasting system for the Oklahoma City area during the Joint Urban 2003 field project. *J Appl Meteorol Clim* 45:912–929
- Martilli A (2007) Current research and future challenges in urban mesoscale modelling. *Int J Climatol* 27(14):1909–1918
- Mlawer EJ, Taubman SJ, Brown PD, Iacono MJ, Clough SA (1997) Radiative transfer for inhomogeneous atmospheres: Rrtm, a validated correlated-k model for the longwave. *J Geophys Res Atmos* 102D:16,663–16,682
- Niyogi D, Holt T, Zhong S, Pyle PC, Basara J (2006) Urban and land surface effects on the 30 July 2003 mesoscale convective system event observed in the southern Great Plains. *J Geophys Res* 111(D19):107
- Pasquill F, Smith FB (1984) Atmospheric diffusion, 3rd edn. John Wiley and Sons Inc, New York, 429 pp
- Salamanca F, Marilli A, Tewari M, Chen F (2011) A study of the urban boundary layer using different urban parameterizations and high-resolution urban canopy parameters with wrf. *J Appl Meteorol Clim* 50:1107–1128
- Stull RB (1988) An introduction to boundary layer meteorology. Kluwer Academic Publishers, Dordrecht, 670 pp
- Tewari M, Kusaka H, Chen F, Coirier WJ, Kim S, Wyszogrodzki AA, Warner TT (2010) Impact of coupling a microscale computational fluid dynamics model with a mesoscale model on urban scale contaminant transport and dispersion. *Atmos Res* 96:656–664
- Thompson G, Field PR, Rasmussen RM, Hall WD (2008) Explicit forecasts of winter precipitation using an improved bulk microphysics scheme. Part II: implementation of a new snow parameterization. *Mon Weather Rev* 136:5095–5115
- Wyszogrodzki AA, Miao S, Chen F (2012) Evaluation of the coupling between mesoscale-wrf and leseulag models for simulating fine-scale urban dispersion. *Atmos Res* 118:324–345
- Xie B, Fung JCH, Chan A, Lau A (2012) Evaluation of nonlocal and local planetary boundary layer schemes in the WRF model. *J Geophys Res* 117(D12):103